

## Marangoni instability in a thin film heated from below: Effect of nonmonotonic dependence of surface tension on temperature

Rajkumar Sarma and Pranab Kumar Mondal\*

*Department of Mechanical Engineering, Indian Institute of Technology Guwahati, Assam, 781039, India*

(Received 9 January 2018; published 9 April 2018)

We investigate Marangoni instability in a thin liquid film resting on a substrate of low thermal conductivity and separated from the surrounding gas phase by a deformable free surface. Considering a nonmonotonic variation of surface tension with temperature, here we analytically derive the neutral stability curve for the monotonic and oscillatory modes of instability (for both the long-wave and short-wave perturbations) under the framework of linear stability analysis. For the long-wave instability, we derive a set of amplitude equations using the scaling  $k \sim (\text{Bi})^{1/2}$ , where  $k$  is the wave number and  $\text{Bi}$  is the Biot number. Through this investigation, we demonstrate that for such a fluid layer upon heating from below, both monotonic and oscillatory instability can appear for a certain range of the dimensionless parameters, viz., Biot number ( $\text{Bi}$ ), Galileo number ( $\text{Ga}$ ), and inverse capillary number ( $\Sigma$ ). Moreover, we unveil, through this study, the influential role of the above-mentioned parameters on the stability of the system and identify the critical values of these parameters above which instability initiates in the liquid layer.

DOI: [10.1103/PhysRevE.97.043105](https://doi.org/10.1103/PhysRevE.97.043105)

### I. INTRODUCTION

Marangoni convection in a fluid layer, which finds applications in areas like thin film evaporators, crystal growth, phase separation process, etc., has been a focus of interest for researchers for the past few decades [1–3]. Originating from the variation of surface tension of fluids, this convection phenomenon is typically encountered in microfluidic systems as well [4–6]. Albeit both the Marangoni and the Bénard (induced by buoyancy) convection can occur in a heated liquid layer, several investigations reveal that for a sufficiently thin layer, Marangoni convection predominates over the Bénard convection [7–10] attributed primarily to the dominance of thermocapillarity over the buoyancy effect. Due to the involvement of the surface effects (surface tension) rather than the volumetric ones (buoyancy), such convection phenomenon can even occur in the microgravity environment as demonstrated by previous researchers in this field [11–14]. However, when both the thermocapillary and buoyancy effects are present together, the phenomenon is collectively called the “Marangoni-Bénard” convection as reported in a number of studies [15–18].

Surface tension is a property of liquids that can vary with temperature, concentration, electrochemical potential, etc. For a pure liquid, the surface tension is a sole function of temperature, whereas for binary fluids, surface tension can vary with both the temperature and concentration of the fluid [19–21]. Therefore, for pure liquids, the Marangoni convection is induced under the sole influence of thermocapillary effect, while, for binary fluids, such convection process occurs by the combined action of thermocapillary and solutocapillary effects

[22–24]. Several experimental investigations reported in the literature suggest that, for most of the fluids, surface tension has a linear relationship with temperature. With an increase in temperature, the surface tension of such fluids decreases monotonically [25]. As such, the literature is rich with the analysis of Marangoni convection for such kind of fluids [9,26,27]. Another important aspect is the nonlinear variation of surface tension with temperature. In this context, we would like to mention here that experiments carried out following well-developed methods reveal that for a certain class of fluids, surface tension varies nonmonotonically with temperature. This particular behavior of surface tension is demonstrated by fluids like long chain aqueous solutions of alcohol, water-oil-surfactant systems, nematic liquid crystals, ionic liquids, etc. [28–33]. These fluids are frequently called “self-rewetting” fluids due to their unique behavior in the boiling process [34]. Several investigations have revealed that such fluids enhance the heat transfer rate in thermal management systems, especially in heat pipes [35–37]. While a series of papers was devoted to the Marangoni convection in a liquid layer with linear dependency of surface tension with temperature [9,27,38,39], considering the nonmonotonic behavior of surface tension with temperature, a few studies on Marangoni convection are available in the literature as well [40–42].

In the study of Marangoni convection in a heated liquid layer resting atop a substrate, generally two cases are considered: conducting and insulating substrates for temperature perturbations [9,43]. For the conducting case, a fixed liquid temperature prevails at the substrate, whereas for the insulating case, the normal component of heat flux remains fixed at the substrate. For both the conducting and insulating substrates (for temperature perturbations), two modes of instability can occur in a liquid layer, viz., the monotonic mode (stationary convection) and the oscillatory mode (overstability) [44–46].

\*mail2pranab@gmail.com

For a liquid layer heated from below, the monotonic mode of instability was first detected by Pearson [9] for both the conducting and insulating substrates. Takashima [47] showed that, for a conducting substrate, an oscillatory mode of instability can also emerge in the liquid layer when heated from above. Recently, for the long-wave perturbations, Shklyaev *et al.* [48] detected the oscillatory mode of instability for a liquid layer resting on an insulating substrate and heated from below. Extending this analysis Samoilova and Lobov [49] discovered the oscillatory modes of instability for the short-wave perturbations. To summarize, the reported studies as mentioned above are focused on the Marangoni convection either in a pure liquid layer or in binary fluids heated from above or below, mainly taking a linear variation of surface tension with temperature into account in the analysis. In particular, the above-mentioned studies concentrated both on the long-wave as well as short-wave oscillatory modes of instability associated with Marangoni convection of a liquid layer resting either on a conducting or an insulating substrate for temperature perturbations. Moreover, it is worth noting that the investigation of long-wave Marangoni convection in a liquid layer lying atop a substrate of low thermal conductivity is generally performed under the well-established asymptotic limits of  $k \sim (\text{Bi})^{1/2}$  and  $k \sim (\text{Bi})^{1/4}$ , where  $k$  and  $\text{Bi}$  are, respectively, the wave number of perturbation and Biot number of the free surface [23,50]. Albeit a significant advancement in investigating the Marangoni instability of a heated liquid layer has been made by the research community, the analysis of such kind of instabilities for both the long-wave and short-wave disturbances considering the nonlinear variation of surface tension with temperature is insufficient to date essentially to explore the physical insights involved with the underlying thermohydrodynamics.

In this study, we have executed an analysis on the Marangoni convection in a heated liquid layer for which surface tension varies nonmonotonically with temperature. Considering the effect of gravity, here, we have theoretically addressed the instabilities of such a fluid layer subjected to both the long-wave and short-wave perturbations.

The paper is organized as follows: We formulate the problem in detail in Sec. II. In Sec. III, we analyze the problem for the long-wave perturbations. Also, Sec. III A is continued with the discussion as follows: Using lubrication approximation and following the scaling  $k \sim (\text{Bi})^{1/2}$ , we demonstrate both the monotonic and oscillatory modes of instability in the heated liquid layer. The problem is analyzed for short-wave perturbations in Sec. III B by demonstrating both the monotonic and oscillatory instability modes. Finally, we make an effort in Sec. IV to summarize the principal conclusions obtained from this analysis.

## II. PROBLEM FORMULATION

We consider a plane incompressible liquid layer with infinite extent in the longitudinal directions  $x$  and  $y$ , and having an unperturbed height  $H$  in the gravitational field  $\mathbf{g}$  as shown in Fig. 1. The liquid layer lies atop a horizontal solid substrate of low thermal conductivity and is bounded above (at the  $z = H$  plane) by a deformable free surface. The entire liquid layer is heated uniformly from below so that a constant vertical

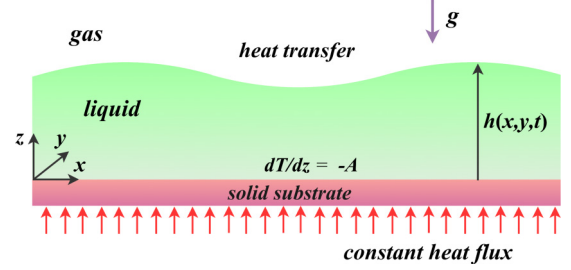


FIG. 1. Schematic of the physical system under consideration with the imposed boundary conditions. The deformable interface is located at  $z = h(x,y,t)$ . A constant heat flux provided at the solid substrate yields the temperature gradient  $-A$  at the  $z = 0$  plane.

temperature gradient  $-A$  prevails at the  $z = 0$  plane. The liquid layer remains at rest up to a certain critical value of  $A$ , above which the Marangoni convection starts appearing in it due to the variation of surface tension ( $\sigma$ ) with temperature ( $T$ ). We assume the unperturbed layer thickness  $H$  to be sufficiently small so that the effect of buoyancy can be neglected as compared to the Marangoni effect. In this analysis, we consider the Marangoni convection to be induced by a nonlinear variation of surface tension with temperature, dictated by the quadratic relationship  $\sigma = \sigma_o - \sigma_T(T - T_\infty)^2/2$  [28]. However, except for surface tension, all other thermophysical properties, viz., the thermal conductivity  $\kappa$ , viscosity  $\mu$ , and density  $\rho$  of the liquid layer are assumed to remain invariant with temperature. We further consider the heat flux from the free surface to be governed by Newton's law of cooling.

### A. Governing equations

For this surface tension driven convection process, the governing transport equations and their associated boundary conditions can be represented in dimensional form by the following set of equations.

Continuity equation:

$$\nabla \cdot \mathbf{v} = 0. \quad (1a)$$

Momentum equation:

$$\mathbf{v}_t + (\mathbf{v} \cdot \nabla)\mathbf{v} = -\rho^{-1}\nabla p + \nu\nabla^2\mathbf{v} - g\mathbf{k}. \quad (1b)$$

Energy equation:

$$T_t + \mathbf{v} \cdot \nabla T = \alpha\nabla^2 T. \quad (1c)$$

In Eqs. (1a)–(1c), the subscript denotes the partial derivative with respect to the corresponding variable,  $\mathbf{v}(\mathbf{u}, w)$  is the velocity field ( $\mathbf{u}$  is the two-dimensional projection of velocity vector onto the  $x$ – $y$  plane and  $w$  is the  $z$  component of velocity),  $p$  is the pressure field, and  $T$  is the temperature field. The terms  $\rho, \nu, \alpha$  in the above equations are, respectively, the fluid density, kinematic viscosity, and thermal diffusivity, while  $g$  represents the gravitational field. Moreover,  $\mathbf{k}$  is the unit vector in the  $z$  direction,  $\nabla \equiv (\partial_x, \partial_y, \partial_z)$ , and  $t$  represents time.

The boundary conditions at the fluid-solid interface (i.e., at the  $z = 0$  plane) are, respectively, the no-slip condition for velocity and a specified heat flux condition.

$$z = 0 : \mathbf{v} = 0, T_z = -A. \quad (2a)$$

At the free surface [i.e., at the  $z = h(x, y, t)$  plane], the boundary conditions represent, respectively, the kinematic boundary condition, heat transfer governed by Newton's law of cooling and the stress balance equation (both normal and tangential stress). Below we write these conditions as

$$z = h(x, y, t) : h_t + \mathbf{u} \cdot \nabla h = w, \quad (2b)$$

$$q(T - T_\infty) = -\kappa(\mathbf{n} \cdot \nabla T), \quad (2c)$$

$$\begin{aligned} & -2\mu\sqrt{1+h_x^2+h_y^2}[u_x(1-h_x^2)+v_y(1-h_y^2)+(u_z+w_x)h_x-(u_y+v_x)h_xh_y+(w_y+v_z)h_y] \\ & = p(1+h_x^2+h_y^2)^{3/2} + \sigma[h_{xx}(1+h_y^2)-2h_xh_yh_{xy}+h_{yy}(1+h_x^2)], \end{aligned} \quad (2d)$$

$$2(w_z - u_x)h_x - (v_z + w_y)h_xh_y - (u_y + v_x)h_y + (u_z + w_x)(1 - h_x^2) = \left(\sqrt{1+h_x^2+h_y^2}/\mu\right)\frac{d\sigma}{dx}, \quad (2e)$$

$$2(w_z - v_y)h_y - (u_z + w_x)h_xh_y - (u_y + v_x)h_x + (v_z + w_y)(1 - h_y^2) = \left(\sqrt{1+h_x^2+h_y^2}/\mu\right)\frac{d\sigma}{dy}. \quad (2f)$$

In Eqs. (2a)–(2f),  $q$  represents the rate of convective heat transfer from the liquid to the ambient gas phase held at fixed temperature  $T_\infty$ ,  $\kappa$  is the thermal conductivity of the liquid,  $\mu$  is dynamic viscosity, and  $\mathbf{n} = (\mathbf{k} - \nabla h)/\sqrt{1 + (\nabla h)^2}$  is the outward unit vector at the gas-liquid interface in the normal direction.

In this study, since our aim is to investigate the effect of nonlinear variation of surface tension (with temperature) on the onset of Marangoni convection, we therefore use the following relationship to represent such variation between the surface tension and the fluid temperature [28]:

$$\sigma = \sigma_o - \sigma_T(T - T_\infty)^2/2. \quad (3)$$

In Eq. (3),  $\sigma_o$  is the surface tension at temperature  $T_\infty$ . Note that such a nonlinear relationship between  $\sigma$  and  $T$  exists for a large class of liquids and can be found in the literature as well [28–30].

### B. Base state

At equilibrium condition, the system under present consideration corresponds to a no-flow condition, indicating a laterally uniform base state. This conductive state of the system can be represented as follows:

$$\begin{aligned} h_o &= H, \quad \mathbf{v}_o = 0, \quad p_o = \rho g(H - z), \\ T_o &= A(H - z) + \frac{\kappa A}{q} + T_\infty. \end{aligned} \quad (4)$$

Before we proceed to investigate the stability of this base state of the system with respect to long-wave and short-wave perturbations, we next try to cast the governing equations

and the associated boundary conditions in a dimensionless framework as discussed in the forthcoming sections.

### C. Dimensionless equations

We now make an effort to nondimensionalize the governing equations and their associated boundary conditions represented by Eqs. (1) and (2). In order to do so, we define the following set of dimensionless variables:

$$\begin{aligned} (\bar{x}, \bar{y}, \bar{z}) &= \frac{(x, y, z)}{H}, \quad \bar{t} = \frac{t}{H^2/\alpha}, \quad (\bar{u}, \bar{v}, \bar{w}) = \frac{(u, v, w)}{\alpha/H} \\ \bar{p} &= \frac{p}{\rho\nu\alpha/H^2}, \quad \bar{T} = \frac{T - T_\infty}{AH}. \end{aligned}$$

Note that, to compare the results of this analysis with that reported in the literature, here we have adopted the same scalings and notations that were used in the earlier studies of Marangoni convection [48,49]. Moreover, for the convenience of presentation, we drop the overbar sign from all the nondimensional variables. Hence the governing equations in dimensionless form read as

Continuity equation:

$$\nabla \cdot \mathbf{v} = 0. \quad (5a)$$

Momentum equation:

$$\text{Pr}^{-1}(\mathbf{v}_t + \mathbf{v} \cdot \nabla \mathbf{v}) = -\nabla p + \nabla^2 \mathbf{v} - \text{Gak}. \quad (5b)$$

Energy equation:

$$T_t + \mathbf{v} \cdot \nabla T = \nabla^2 T. \quad (5c)$$

The associated boundary conditions become

$$z = 0: \quad \mathbf{v} = 0, \quad T_Z = -1, \quad (6a)$$

$$z = h(x, y, t): \quad h_t + uh_x + vh_y = w, \quad (6b)$$

$$(\mathbf{n} \cdot \nabla T) = -\text{Bi}T, \quad (6c)$$

$$\begin{aligned}
 & -2\sqrt{1+h_x^2+h_y^2}[u_x(1-h_x^2)+v_y(1-h_y^2)+(u_z+w_z)h_x-(u_y+v_x)h_xh_y+(w_y+v_z)h_y] \\
 & = p(1+h_x^2+h_y^2)^{3/2}+\Sigma[h_{xx}(1+h_x^2)-2h_xh_yh_{xy}+h_{yy}(1+h_x^2)], \tag{6d}
 \end{aligned}$$

$$2(w_z-u_x)h_x-(v_z+w_y)h_xh_y-(u_y+v_x)h_y+(u_z+w_x)(1-h_x^2)=-\text{Ma}TT_x\sqrt{1+h_x^2+h_y^2}, \tag{6e}$$

$$2(w_z-v_y)h_y-(u_z+w_x)h_xh_y-(u_y+v_x)h_x+(v_z+w_y)(1-h_y^2)=-\text{Ma}TT_y\sqrt{1+h_x^2+h_y^2}. \tag{6f}$$

#### D. Dimensionless base state

In dimensionless form, the base state [see Eq. (4)] can be represented by the following relationships:

$$h_o = 1, \quad \mathbf{v}_o = 0, \quad T_o = 1 - z + \frac{1}{\text{Bi}}, \quad p_o = \text{Ga}(1 - z). \tag{7}$$

Note that the boundary value problem represented by Eqs. (5) and (6) is characterized by the following sets of dimensionless parameters,

$$\begin{aligned}
 \text{Bi} &= \frac{qH}{\kappa}, \quad \text{Ga} = \frac{gH^3}{\nu\alpha}, \quad \text{Ma} = \frac{\sigma_T A^2 H^3}{\rho\nu\alpha}, \\
 \text{Pr} &= \frac{\nu}{\alpha}, \quad \Sigma = \frac{\sigma_o H}{\rho\nu\alpha},
 \end{aligned}$$

which are, respectively, the Biot number, Galileo number, Marangoni number, Prandtl number, and dimensionless surface tension (or inverse capillary number). Here, it is important to note that except for the Marangoni number (Ma), all other nondimensional parameters are defined in the same manner as that in Shklyaev *et al.* [48] and Samoilova and Lobov [49]. However, for this analysis, since we have considered the surface tension to vary nonlinearly with temperature, we therefore define Ma in a slightly different manner and name it the quadratic Marangoni number. Compared to the linear Marangoni number (defined as  $\text{Ma}_L = \sigma_T A H^2 / \rho\nu\chi$  for fluids whose surface tension varies linearly with temperature) the important feature of this quadratic Marangoni number is that, for  $\sigma_T > 0$ , the latter is always a positive quantity (and hence independent of the direction of heating). However,  $\text{Ma}_L$  can be either positive or negative depending on the direction of heating (even for  $\sigma_T > 0$ ).

We now proceed to study the stability of this base state against the long-wave and short-wave perturbations, as discussed systematically in the forthcoming sections.

### III. RESULTS AND DISCUSSION

#### A. Long-wave stability theory

##### 1. Lubrication approximation

In this section, we study the stability of the base state [see Eq. (7)] against the long-wave disturbances. In order to analyze the evolution of such large scale flows, here we use the lubrication approximation. As such, following this approximation, we rescale the coordinates, time, and velocity

as given below:

$$\begin{aligned}
 X &= \varepsilon x, \quad Y = \varepsilon y, \quad Z = z, \quad \tau = \varepsilon^2 t, \\
 u &= \varepsilon U, \quad v = \varepsilon V, \quad w = \varepsilon^2 W.
 \end{aligned} \tag{8}$$

where  $\varepsilon$  is a small parameter ( $0 < \varepsilon \ll 1$ ) and can be considered as the ratio of  $H$  to the longitudinal length scale.

It is important to note that, since the present study is concerned with a liquid layer with poorly conducting boundaries, therefore the magnitude of the Biot number (Bi) must have to be very small ( $\text{Bi} < 1$ ). Moreover, throughout the analysis, we have considered the inverse capillary number ( $\Sigma$ ) to be large [24]. Thus, we can rescale both Bi and  $\Sigma$  in the manner as given below:

$$\text{Bi} = \varepsilon^2 b, \quad \Sigma = \varepsilon^{-2} \zeta. \tag{9}$$

It may be noted that the scaling adopted in Eq. (9) differs from the conventional scaling  $\text{Bi} = O(\varepsilon^4)$ , which is typically used in the study of long-wave Marangoni convection of a liquid layer with insulating boundaries [22,51]. A different scaling is employed in this analysis accounting for the fact that the conventional scaling becomes inadequate at certain situations as demonstrated by Podolny *et al.* [52]. Accordingly, in this analysis, we deal with the intermediate asymptote between the conventional long-wave mode  $\text{Bi} = O(\varepsilon^4)$  and the case of finite Bi, that corresponds to  $b \rightarrow 0$  and  $b \rightarrow \infty$ , respectively. However, it should be mentioned here that, in the present study, we do not impose any restriction on the magnitude of the Galileo number (Ga). Depending upon the strength of the gravitational field, fluid layer thickness, and its properties, Ga can vary from ultralow to a very high value. For instance, under normal gravity condition and for a 0.1-mm-thick layer of water-based solution Ga becomes  $O(10^2)$ , while in microgravity condition, where  $g = O(10^{-2} \text{ m/s}^2)$ ,  $\text{Ga} \sim O(10^{-1})$ .

We now expand all the dependent variables of the problem in a power series with respect to  $\varepsilon^2$  as follows:

$$(U, V, W) = (U_0, V_0, W_0) + \varepsilon^2(U_1, V_1, W_1) + \dots, \tag{10a}$$

$$p = P_0 + \varepsilon^2 P_1 + \dots, \tag{10b}$$

$$T = -Z + \frac{1}{\varepsilon^2 b} + T_0 + \varepsilon^2 T_1 + \dots. \tag{10c}$$

It may be noted here that, in Eq. (10), we have not presented an expansion for  $h$ . This is because the scaling provided by Eq. (8) is sufficient to ensure a slow variation of  $h$ , which further provides a small amplitude of surface deformation [53].

A comparison between Eqs. (7) and (10) reveals that the base state of the system corresponds to  $P_0 = p_o$ ,  $T_0 = 1$ .

Substituting the rescaled fields [Eqs. (8)–(10)] into Eqs. (5) and (6), and applying the conventional technique of lubrication approximation, we obtain the following set of equations:

$$U_{0X} + V_{0Y} + W_{0Z} = 0, \quad (11a)$$

$$P_{0X} = U_{0ZZ}, \quad P_{0Y} = V_{0ZZ}, \quad P_{0Z} = -\text{Ga}, \quad (11b)$$

$$T_{0ZZ} = 0, \quad (11c)$$

$$\text{at } Z = 0: U_0 = V_0 = W_0 = 0, T_{0Z} = 0, \quad (12a)$$

$$\text{at } Z = h(X, Y, \tau): W_0 = h_\tau + U_0 h_X + V_0 h_Y, \quad T_{0Z} = 0,$$

$$U_{0Z} = -\text{Ma} \left( T_0 + \frac{1}{\varepsilon^2 b} - h \right) (T_{0X} - h_X), \quad (12b)$$

$$V_{0Z} = -\text{Ma} \left( T_0 + \frac{1}{\varepsilon^2 b} - h \right) (T_{0Y} - h_Y),$$

$$-P_0 = \zeta (h_{XX} + h_{YY}).$$

The solutions of Eqs. (11a)–(11c), subjected to the boundary conditions as given in Eqs. (12a) and (12b), can be written as

$$U_0 = \frac{1}{2} Z(Z - 2h) \partial_X [\text{Gah} - \zeta \nabla^2 h] - \text{Ma} Z \left( \theta + \frac{1}{\varepsilon^2 b} - h \right) (\theta_X - h_X), \quad (13a)$$

$$V_0 = \frac{1}{2} Z(Z - 2h) \partial_Y [\text{Gah} - \zeta \nabla^2 h] - \text{Ma} Z \left( \theta + \frac{1}{\varepsilon^2 b} - h \right) (\theta_Y - h_Y), \quad (13b)$$

$$W_0 = \frac{1}{2} Z^2 \nabla \cdot \left[ \frac{1}{3} (3h - Z) \nabla \mathfrak{S} + \text{Ma} \mathfrak{R} \right], \quad (13c)$$

$$P_0 = \text{Ga}(h - Z) - \zeta \nabla^2 h, \quad (13d)$$

$$T_0 = \theta(X, Y, \tau), \quad (13e)$$

where  $\mathfrak{S} = \text{Gah} - \zeta \nabla^2 h$  and  $\mathfrak{R} = \left( \theta + \frac{1}{\varepsilon^2 b} - h \right) \nabla (\theta - h)$ .

In Eqs. (13a)–(13e),  $\nabla \equiv (\partial_X, \partial_Y, 0)$  is the two-dimensional projection of the gradient operator onto the  $X$ – $Y$  plane. Here, the base state, which corresponds to the motionless state of the liquid layer, is given by

$$h = 1, \quad \theta = 1. \quad (14)$$

In what follows, we study the stability of this base state of the system with respect to infinitesimal perturbations as discussed in the subsequent sections.

## 2. Amplitude equations

In order to obtain the first amplitude equation, we use the condition  $h_\tau = -\nabla \cdot \int_0^h \mathbf{U}_0 dZ$  which governs the evolution of the fluid layer thickness. This condition gives the following

expression as

$$h_\tau = \nabla \cdot \left[ \frac{1}{3} h^3 \nabla \mathfrak{S} + \frac{1}{2} \text{Ma} h^2 \mathfrak{R} \right]. \quad (15)$$

The first term on the right-hand side of Eq. (15) takes into account the damping effect of gravity as well as the surface tension on the surface deflection of the liquid layer, while the second term represents the influence of thermocapillarity induced flow on the liquid layer.

It may be mentioned here that the second amplitude equation is obtained from the heat transfer equation. Following the first order expansion of Eq. (5c) and the associated boundary conditions [Eqs. (6a) and (6c)], we get the following set of equations as described below:

$$T_{1ZZ} = \theta_\tau + U_0 T_{0X} + V_0 T_{0Y} - \nabla^2 \theta - W_0, \quad (16)$$

$$\text{at } Z = 0: T_{1Z} = 0, \quad (17a)$$

$$\text{at } Z = h(X, Y, \tau): T_{1Z} = \nabla \theta \cdot \nabla h - \frac{1}{2} (\nabla h)^2 - b(\theta - h). \quad (17b)$$

Integration of Eq. (16) subjected to the boundary conditions as given in Eqs. (17a) and (17b) provides the second amplitude equation. Below we write the second amplitude equation as

$$h\theta_\tau = \nabla \cdot \left( \frac{1}{8} h^4 \nabla \mathfrak{S} + \frac{1}{6} \text{Ma} \mathfrak{R} h^3 \right) + \left( \frac{1}{3} h^3 \nabla \mathfrak{S} + \frac{1}{2} \text{Ma} \mathfrak{R} h^2 \right) \cdot \nabla (\theta - h) + \nabla \cdot (h \nabla \theta) - \frac{1}{2} (\nabla h)^2 - b(\theta - h). \quad (18)$$

The first two terms on the right-hand side of Eq. (18) take into account the advective transport of heat by the fluid; the third term represents the heat conductivity in the longitudinal directions, while the last two terms take care of the heat loss from the free surface. As such, the set of amplitude equations [Eqs. (15) and (18)] governs the nonlinear dynamics of the long-wave perturbations.

## 3. Linear stability analysis

The amplitude equations, given in Eqs. (15) and (18) are nonlinear in  $h$  and  $\theta$ . We here make an effort to linearize these equations using small perturbation analysis. Substituting the perturbed fields, viz.,  $h = 1 + \delta$  and  $\theta = 1 + \phi$ , and linearizing the equations with respect to small disturbances we get the following expressions as

$$\delta_\tau = \nabla^2 \left[ \frac{1}{3} (\text{Ga} \delta - \zeta \nabla^2 \delta) + \frac{1}{2} \frac{\text{Ma}}{\varepsilon^2 b} (\phi - \delta) \right], \quad (19a)$$

$$\phi_\tau = \nabla^2 \left[ \phi + \frac{1}{8} (\text{Ga} \delta - \zeta \nabla^2 \delta) + \frac{1}{6} \frac{\text{Ma}}{\varepsilon^2 b} (\phi - \delta) \right] - b(\phi - \delta). \quad (19b)$$

Now, representing the perturbation fields to be proportional to  $\exp(iKX + \lambda\tau)$  where  $K$  and  $\lambda (= \lambda_r + i\lambda_i)$  are, respectively, the dimensionless wave number and complex growth rate of the perturbations, we arrive at the following dispersion

relation as mentioned next.

$$\lambda^2 + (\lambda/3)[3b + K^2(3 + Ga + \zeta K^2 - Ma/\varepsilon^2 b)] - (K^2/144\varepsilon^2 b)[MaK^2(72 + Ga + \zeta K^2)] + (K^2/3)[(b + K^2)(Ga + \zeta K^2)] = 0. \quad (20)$$

It may be noted that Eq. (20) possesses both the real and complex solutions. The real solution of Eq. (20) represents the monotonic instability, whereas the complex solution corresponds to the oscillatory instability. We next discuss both kinds of (monotonic and oscillatory) instabilities systematically in the subsequent sections.

**4. Monotonic instability**

We first start with the case of monotonic instability. At the monotonic instability threshold, the disturbance growth rate ( $\lambda$ ) vanishes [43]. Substituting  $\lambda = 0$  in Eq. (20), we arrive at the relationship that determines the monotonic instability boundary as

$$Ma_m = \frac{48\varepsilon^2 b(b + K^2)(Ga + \zeta K^2)}{K^2(72 + Ga + \zeta K^2)}. \quad (21)$$

In terms of the unscaled wave number  $k(= \varepsilon K)$ , Biot number (Bi), and inverse capillary number ( $\Sigma$ ), Eq. (21) can be reproduced in the following form as

$$Ma_m = \frac{48Bi(Bi + k^2)(Ga + \Sigma k^2)}{k^2(72 + Ga + \Sigma k^2)}. \quad (22)$$

For a nondeformable free surface (i.e., for  $Ga + \Sigma k^2 \gg 72$ ) at large  $k$ , Eq. (22) reduces to the following:

$$Ma_m = 48Bi. \quad (23)$$

**5. Oscillatory instability**

The oscillatory instability boundary is determined by the condition where the disturbance growth rate ( $\lambda$ ) attains a purely imaginary value  $\lambda = i\lambda_i$ . Here,  $\lambda_i$  is the oscillation frequency and is a real quantity. The neutral stability curve for the oscillatory instability mode is given by the following expression as

$$Ma_o = \varepsilon^2 b \left( 3 + \frac{3b}{K^2} + Ga + \zeta K^2 \right), \quad (24)$$

and the oscillation frequency is determined by the relation

$$\lambda_i = K^2 \sqrt{(72 + Ga + \zeta K^2)(Ma_o - Ma_m)/144Bi}. \quad (25)$$

For the unscaled wave number  $k(= \varepsilon K)$ , Biot number (Bi), and inverse capillary number ( $\Sigma$ ), we can rewrite Eq. (24) as

$$Ma_o = Bi \left( 3 + \frac{3Bi}{k^2} + Ga + \Sigma k^2 \right). \quad (26)$$

It is important to mention here that the oscillatory mode of instability takes place only when  $Ma_o(k) < Ma_m(k)$ .

We present the neutral stability curves for the long-wave monotonic and oscillatory modes of instability in Fig. 2. For numerical calculations, consistent with the assumptions

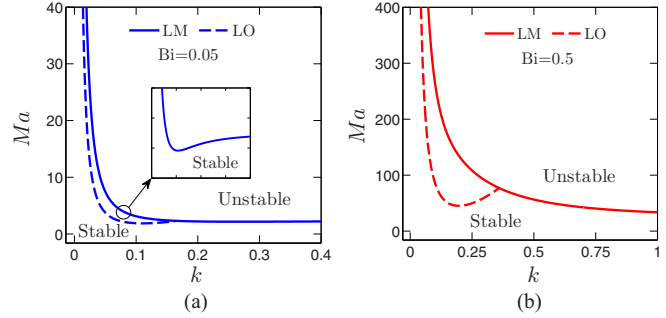


FIG. 2. Neutral stability curves for the long-wave monotonic (solid lines) and oscillatory (dashed lines) modes at  $Pr = 1$ ,  $Ga = 10$ , and  $\Sigma = 1000$ . Panel (a) corresponds to  $Bi = 0.05$ ; (b) corresponds to  $Bi = 0.5$ . The inset in (a) shows the zoomed-in view of the stability curve for the monotonic mode of instability.

considered in the analysis, we use the following range for the parameters  $Bi$ ,  $\Sigma$ , and  $Ga$  [49]:

$$O(10^{-3}) \lesssim Bi \lesssim O(10^{-1}), \quad O(10^2) \lesssim \Sigma \lesssim O(10^4), \\ O(1) \lesssim Ga \lesssim O(10).$$

Moreover, throughout the analysis, we have taken following the values used in several studies in this field [24,54]  $Pr \sim O(1)$ , which is consistent with the typical values for most of the fluids as well.

From Fig. 2 it can be observed that, for both the monotonic and oscillatory modes of instability, there exists a minimum Marangoni number only above which the instability first appears in the liquid layer. Henceforth, we call this Marangoni number as the critical Marangoni number ( $Ma_c$ ) and the disturbance wave number ( $k$ ) associated with this  $Ma_c$  as the critical wave number ( $k_c$ ). Figures 2(a) and 2(b) also demonstrate the effect of Biot number (Bi) on the stability of the system. A closer observation of Figs. 2(a) and 2(b) reveals that the critical Marangoni number ( $Ma_c$ ) of the system increases with an increase in the magnitude of the Biot number (Bi). This observation signifies that the higher values of Bi enhance the stability of the system. It is important to note that, in this analysis, Bi characterizes the heat loss from the free surface of the liquid layer. Therefore, the higher is the magnitude of Bi, the higher will be the heat transfer rate from the free surface of the liquid. This increased heat transfer rate from the free liquid surface increases the stability of the system for higher values of Bi as witnessed in Figs. 2(a) and 2(b). Moreover, Fig. 2 further demonstrates that for  $Bi = 0.05$  the oscillatory mode is critical, whereas for  $Bi = 0.5$  the monotonic mode becomes critical. A detailed discussion on the variation of the instability modes with Biot number is provided later in the context of the discussion of Figs. 6 and 7.

For finite values of  $k$ , Eq. (22) indicates that the neutral stability curve for the long-wave monotonic mode has a minimum Marangoni number ( $Ma = Ma_c$ ) when  $Bi\Sigma < 72$ . This is also confirmed from the inset of Fig. 2(a). The critical wave number ( $k_c$ ) and the critical Marangoni number ( $Ma_c$ ) corresponding to this minimum of the neutral stability curve

are given by Eqs. (27) and (28), respectively.

$$k_{c,m} = \sqrt{\frac{\text{BiGa}\Sigma + \sqrt{\text{Bi}^2\text{Ga}^2\Sigma^2 + \text{BiGa}\Sigma(72 + \text{Ga})(72 - \text{Bi}\Sigma)}}{\Sigma(72 - \text{Bi}\Sigma)}}, \tag{27}$$

and

$$\text{Ma}_{c,m} = \frac{48\text{Bi}[\Pi + \text{Bi}\Sigma(72 - \text{Bi}\Sigma)][\text{Ga}(72 - \text{Bi}\Sigma) + \Pi]}{\Pi[(72 - \text{Bi}\Sigma)(72 + \text{Ga}) + \Pi]}, \tag{28}$$

where  $\Pi = \text{BiGa}\Sigma + \sqrt{\text{Bi}^2\text{Ga}^2\Sigma^2 + \text{BiGa}\Sigma(72 + \text{Ga})(72 - \text{Bi}\Sigma)}$ .

However, for  $\text{Bi}\Sigma > 72$ , the minimum of this neutral stability curve occurs at  $\text{Ma}_c = 48\text{Bi}$  in the limit of  $k \rightarrow \infty$  as can be verified from Fig. 2(b).

The neutral stability curve for the long-wave oscillatory mode also presents a minimum as can be observed from Fig. 2. Below, in Eq. (29), we provide the critical Marangoni number ( $\text{Ma}_{c,o}$ ) and disturbance wave number ( $k_{c,o}$ ) corresponding to this minimum of the neutral stability curve.

$$\text{Ma}_{c,o} = \text{Bi}(3 + \text{Ga} + 2\sqrt{3\text{Bi}\Sigma}), \quad k_{c,o} = \left(\frac{3\text{Bi}}{\Sigma}\right)^{1/4}. \tag{29}$$

The variations of the critical Marangoni number and the critical wave number for both the monotonic and oscillatory modes of instability with the dimensionless parameters  $\text{Bi}$ ,  $\text{Ga}$ , and  $\Sigma$  are presented in Sec. II B.

We demonstrate, in Fig. 3, the effect of Galileo number ( $\text{Ga}$ ) on the stability of the system. In this analysis, since  $\mathbf{g}$  is nondimensionalized as  $\text{Ga}$ , therefore Fig. 3 basically addresses the effect of gravity on the stability of the liquid layer. From Fig. 3, it can be observed that increasing the magnitude of  $\text{Ga}$  increases the stability of the system. This is because of the

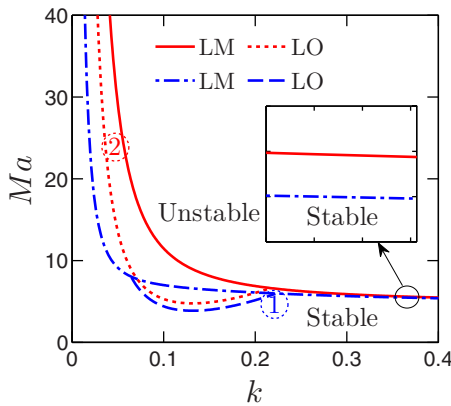


FIG. 3. Neutral stability curves for the long-wave monotonic (solid and dash-dotted lines) and oscillatory modes (dotted and dashed lines) for different values of  $\text{Ga}$  at  $\text{Pr} = 1$ ,  $\Sigma = 1000$ , and  $\text{Bi} = 0.1$ . Lines marked by 1 and 2 correspond to  $\text{Ga} = 1$  and  $\text{Ga} = 10$ , respectively. The inset shows the zoomed-in view of the stability curve at higher wave number.

fact that, for higher values of  $\text{Ga}$ , the stabilizing influence of gravity dominates over the destabilizing effect introduced in the system by the effect of thermocapillarity, thus leading to an enhancement in the stability of the system for higher values of Galileo number as witnessed from Fig. 3. However, the increasing magnitude of Galileo number reduces the range of disturbance wave number ( $k$ ) for which the oscillatory mode is critical as can be observed from Fig. 3.

Figure 4 depicts the effect of  $\Sigma$  (inverse capillary number) on the stability of the system under consideration in this analysis. In this study, since  $\Sigma$  represents the nondimensional surface tension, therefore Fig. 4 essentially demonstrates the effect of surface tension on the stability of the liquid layer. From Fig. 4 it can be observed that the increasing magnitude of  $\Sigma$  enhances the stability of the system. We attribute this observation to the influential role of surface tension on the stability of the liquid layer. In this context, it may be mentioned that the surface tension is a fluid property that tries to stabilize a system by dampening the surface deflections. Hence, increasing the magnitude of surface tension (and thus  $\Sigma$ ) increases the stability of the fluid layer by reducing the surface deformations as can be verified from Fig. 4. However, the higher values of  $\Sigma$  reduce the range of disturbance wave number ( $k$ ) that is also observed in Fig. 4, for which the oscillatory mode is critical.

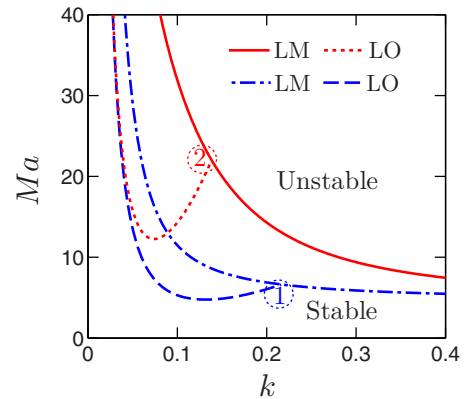


FIG. 4. Neutral stability curves for the long-wave monotonic (solid and dash-dotted lines) and oscillatory modes (dotted and dashed lines) for different  $\Sigma$  at  $\text{Pr} = 1$ ,  $\text{Ga} = 10$ , and  $\text{Bi} = 0.1$ . Lines marked by 1 and 2 correspond to  $\Sigma = 1000$  and  $\Sigma = 10000$ , respectively.

**B. Short-wave stability theory**

In this section, we investigate the short-wave mode of Marangoni instability induced by the nonlinear variation of surface tension with temperature.

**1. Linear stability analysis**

Here, we study the stability of the base state of the system [see Eq. (7)] with respect to the short-wave perturbations. Since the problem under present consideration is invariant of the rotation of the system in the  $x-y$  plane, therefore we consider two-dimensional infinitesimal perturbations only in the  $x-z$  plane for analyzing the stability of the base state. Substituting the perturbed fields  $\mathbf{v} = (u, 0, w)$ ,  $p = p_0 + P$ ,  $T = T_0 + \theta$ , and  $h = 1 + \xi$ , and linearizing Eqs. (5) and (6) with respect to these small disturbances, we get the following set of equations:

$$\nabla \cdot \mathbf{v} = 0, \tag{30a}$$

$$\text{Pr}^{-1} \mathbf{v}_t = -\nabla P + \nabla^2 \mathbf{v}, \tag{30b}$$

$$\theta_t = \nabla^2 \theta + w, \tag{30c}$$

$$\text{at } z = 0: \mathbf{v} = 0, \theta_z = 0, \tag{31a}$$

$$\text{at } z = 1: \xi_t = w, P - \text{Ga}\xi = -\Sigma \xi_{xx} + 2w_z,$$

$$u_z + w_x = -\text{Ma}(\theta_x - \xi_x)/\text{Bi}, \theta_z = -\text{Bi}(\theta - \xi). \tag{31b}$$

Now, utilizing the stream function relations  $u = \psi_z$  and  $w = -\psi_x$ , we can write Eqs. (30) and (31) in the following form:

$$\text{Pr}^{-1} \frac{\partial \nabla^2 \psi}{\partial t} = \nabla^4 \psi, \tag{32a}$$

$$\theta_t = \nabla^2 \theta - \psi_x, \tag{32b}$$

$$\text{at } z = 0: \psi = 0, \psi_z = 0, \theta_z = 0, \tag{33a}$$

$$\text{at } z = 1: \xi_t = -\psi_x,$$

$$P - \text{Ga}\xi = -\Sigma \xi_{xx} - 2 \frac{\partial^2 \psi}{\partial x \partial z}, \tag{33b}$$

$$\psi_{zz} - \psi_{xx} = -\text{Ma}(\theta_x - \xi_x)/\text{Bi}, \theta_z = -\text{Bi}(\theta - \xi).$$

Representing the perturbation fields to be proportional to  $\exp(-\lambda t + ikx)$ , where  $\lambda (= \lambda_r + i\lambda_i)$  and  $k$  are, respectively, the disturbance growth rate and disturbance wave number, Eqs. (32) and (33) become

$$\psi^{iv} - \left(2k^2 - \frac{\lambda}{\text{Pr}}\right) \psi'' + \left(k^2 - \frac{\lambda}{\text{Pr}}\right) k^2 \psi = 0, \tag{34a}$$

$$\theta'' + (\lambda - k^2) \theta = ik\psi, \tag{34b}$$

$$\text{at } z = 0: \psi = 0, \psi' = 0, \theta' = 0, \tag{35a}$$

$$\text{at } z = 1: \lambda \xi = ik\psi, \psi''' - \left(3k^2 - \frac{\lambda}{\text{Pr}}\right) \psi'$$

$$= ik(\text{Ga} + \Sigma k^2) \xi,$$

$$\psi'' + k^2 \psi = -ik\text{Ma}(\theta - \xi)/\text{Bi}, \theta' = -\text{Bi}(\theta - \xi). \tag{35b}$$

In Eqs. (34) and (35) the prime denotes the  $z$  derivative, and the superscript  $iv$  represents the fourth order derivative.

**2. Monotonic instability**

It is mentioned earlier that, for the monotonic mode of instability,  $\lambda = 0$  at the stability border. Substituting  $\lambda = 0$  in Eqs. (34) and (35) and solving for  $\psi$  and  $\theta$ , we obtain the following expressions:

$$\psi = a_1 \sinh kz - a_1 kz \cosh kz + a_2 kz \sinh kz, \tag{36}$$

$$\theta = \frac{i}{4k} [3a_1 kz \cosh kz - 3a_1 \sinh kz - a_1 k^2 z^2 \sinh kz + a_2 k^2 z^2 \cosh kz - a_2 kz \sinh kz + a_3 \cosh kz]. \tag{37}$$

Note that the above solutions for  $\psi$  and  $\theta$  are obtained by applying the boundary conditions at the  $z = 0$  plane. Substituting the boundary conditions at  $z = 1$  into the solution of  $\psi$  and  $\theta$ , and solving for  $\text{Ma}$ , we get the following expression for the neutral stability curve:

$$\text{Ma}_m = \frac{8k\text{Bi}(\text{Ga} + \Sigma k^2)(\cosh k \sinh k - k)(k \sinh k + \text{Bi} \cosh k)}{(\text{Ga} + \Sigma k^2)(\cosh k \sinh^2 k - 2k \sinh k + k^2 \cosh k - k^3 \sinh k) + 8k^5 \sinh k}. \tag{38}$$

It is worth noting that, for the limit  $k \ll 1$ ,  $\text{Bi} \sim k^2$ , and  $\Sigma \sim k^{-2}$ , Eq. (38) resembles Eq. (22).

**3. Oscillatory instability**

For the oscillatory mode of instability  $\lambda_i \neq 0$  at the stability border. Solving Eqs. (34) and (35) using the boundary conditions at  $z = 0$ , we get the solution for  $\psi$  and  $\theta$  as given below:

$$\psi = -c_1(k_1) \sinh kz + c_1 \sinh k_1 z - c_2 \cosh kz + c_2 \cosh k_1 z, \tag{39}$$

$$\theta = \frac{i}{2\lambda k_1 k_2} \left[ \begin{aligned} &-2k c_1 k_1^2 \exp(-k_2 z) + k \lambda c_1 \exp(-k_2 z) - 2c_1 k_1^2 k_2 \sinh k z + \lambda c_1 k k_2 z \cosh k_1 z \\ &-2k k_1 c_2 k_2 \cosh k z + \lambda c_2 k k_2 z \sinh k_1 z + 2\lambda k_1 k_2 c_3 \cosh k_2 z \end{aligned} \right]. \tag{40}$$

Employing the boundary conditions at  $z = 1$  in the solution of  $\psi$  and  $\theta$ , and solving for  $Ma$ , we obtain the following expression that governs the neutral stability curve for the short-wave oscillatory mode of instability.

$$Ma_o = \frac{\aleph_1 \aleph_4 + \aleph_0 \aleph_1 \aleph_5}{\aleph_1 \aleph_6 + \aleph_2 \aleph_8 + \aleph_0 \aleph_1 \aleph_7 + \aleph_0 \aleph_3 \aleph_8}. \tag{41}$$

The quantities  $\aleph_0 - \aleph_8$  appearing in Eq. (41) are lengthy. For brevity in presentation we do not provide these expressions here; rather they are defined in the Appendix of this paper.

We show in Fig. 5 the neutral stability curve for the monotonic and oscillatory modes of instability obtained at different Biot numbers ( $Bi$ ). From Figs. 5(a) and 5(b) it can be observed that, with increasing the magnitude of  $Bi$ , following a similar trend with the long-wave mode, the stability of the liquid layer also increases for the short-wave mode. A detailed discussion on the influence of Biot number on the stability of the system is provided earlier in the context of discussion of Fig. 2. Moreover, Fig. 5 also compares the results between the long-wave and short-wave stability analysis. We observe that, for  $Bi = 0.05$ , the results of the long-wave analysis agree well with the short-wave analysis for all the range of wave number ( $k$ ) considered in this analysis, while for  $Bi = 0.5$ , the results between long-wave and short-wave analysis match only for small values of  $k$ . It is worth mentioning here that the observations as reflected in Fig. 5 show similarity with those reported in the literature [49].

Figures 6(a) and 6(b) depict the variation of the critical Marangoni number ( $Ma_c$ ) and the disturbance wave number ( $k_c$ ) with Biot number ( $Bi$ ). It is observed that the stability of the system increases with increasing magnitude of  $Bi$  as indicated by an increase in  $Ma_c$  for higher values of Biot number. Moreover, Fig. 6(a) further demonstrates that there exists a particular range of  $Bi$  only within which the oscillatory mode (for both the long-wave and short-wave perturbations) becomes critical [see inset of Fig. 6(a)]. It is worth mentioning that this range depends on the magnitude of both  $Ga$  and  $\Sigma$ , as

can be found from Figs. 7(a) and 7(b). However, outside this range, the monotonic mode becomes critical, which is also observed from the present figures (Figs. 6 and 7).

A closer look at Figs. 6(a) and 6(b) further reveals that the results of the long-wave stability analysis agree well with the short-wave analysis for small values of  $Bi$ . For the monotonic mode of instability, this range is  $0 < Bi < 0.072$  corresponding to  $0 < Bi\Sigma < 72$ . Moreover, for the monotonic mode of instability, the critical wave number ( $k_c$ ) for the long-wave approximation agrees with the short-wave analysis in a fairly accurate manner up to the range  $Bi < 0.072$ , as can be seen from Fig. 6(b). However, for  $Bi > 0.072$ ,  $k_c$  associated with the long-wave monotonic mode grows rapidly [see Fig. 6(b)], thus limiting the domain of applicability of long-wave approximation.

Figure 8 demonstrates the influence of gravity (here nondimensionalized as the Galileo number,  $Ga$ ) on the stability of the system for the short-wave perturbations. It can be observed that the stability of the system increases with increasing the magnitude of  $Ga$ , attributed primarily to the stabilizing role of gravity on the stability of the heated fluid layer. However, higher values of  $Ga$  reduce the range of disturbance wave number ( $k$ ) for which the oscillatory mode is critical as witnessed in the present figure.

We depict in Fig. 9 the variation of critical Marangoni number ( $Ma_c$ ) and disturbance wave number ( $k_c$ ) with Galileo number ( $Ga$ ). From the present figure it can be observed that, for both the long-wave and short-wave perturbations, the stability of the system increases with increasing the magnitude of  $Ga$ . This is indicated by an increase in  $Ma_c$  for higher values of  $Ga$ . Figure 9(a) further demonstrates that the oscillatory

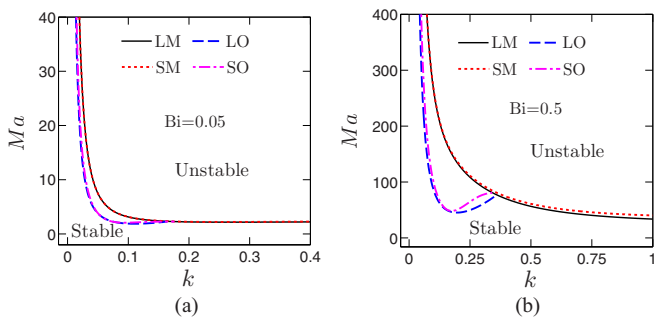


FIG. 5. Neutral stability curves for the monotonic and oscillatory modes of instability at  $Pr = 1$ ,  $Ga = 10$ , and  $\Sigma = 1000$ . Panel (a) corresponds to  $Bi = 0.05$ ; (b) corresponds to  $Bi = 0.5$ . (a), (b) LM, LO, SM, and SO represents the stability curves for the long-wave monotonic, long-wave oscillatory, short-wave monotonic, and short-wave oscillatory modes, respectively.

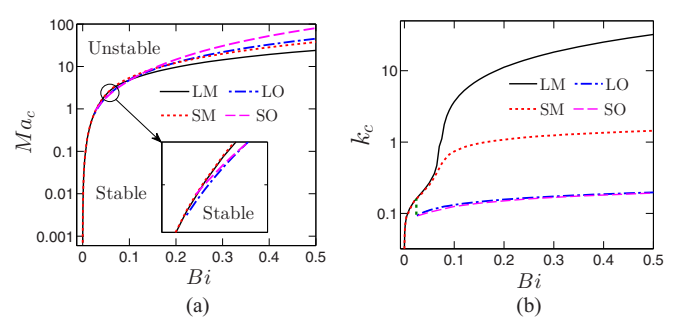


FIG. 6. Variation of the (a) critical Marangoni number, and (b) the critical wave number with  $Bi$  at  $Pr = 1$ ,  $Ga = 10$ , and  $\Sigma = 1000$ . (a), (b) LM, LO, SM, and SO represent the long-wave monotonic, long-wave oscillatory, short-wave monotonic, and short-wave oscillatory modes, respectively. The inset in (a) shows the zoomed-in view at small Biot number.

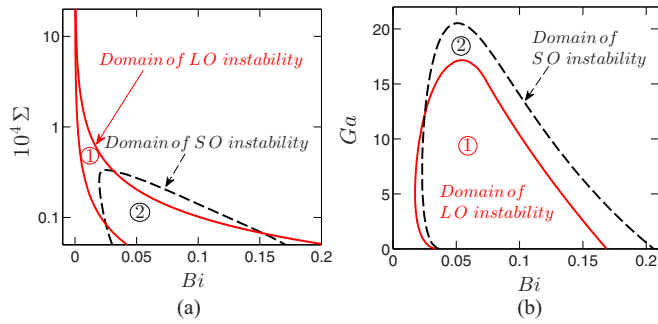


FIG. 7. Variation in the domain of oscillatory instability for (a)  $\Sigma$  vs  $Bi$  at  $Pr = 1$ ,  $Ga = 10$ , and (b)  $Ga$  vs  $Bi$  at  $Pr = 1$ ,  $\Sigma = 1000$ . Domains 1 and 2 in (a), (b) correspond to the long-wave oscillatory (LO) and short-wave oscillatory (SO) modes, respectively.

mode (for both long-wave and short-wave perturbations) is critical only up to a particular value of  $Ga$  ( $\approx 17$ ), after which the monotonic mode becomes critical. Since the increasing magnitude of  $Ga$  reduces the deformability of the free surface, this ensures the fact that for pure Marangoni convection, the oscillatory instability occurs only for a fluid layer having a deformable surface.

The variation of the critical wave number ( $k_c$ ) with  $Ga$  is shown in Fig. 9(b). It can be observed that  $k_c$  for the monotonic mode of instability (for both the long-wave and shortwave perturbations) increases with  $Ga$ . However, for the oscillatory mode,  $k_c$  is independent of  $Ga$  for both the long-wave and short-wave perturbations as can be seen from Fig. 9(b). As such, this observation can be verified by having a closer look at Eq. (29).

Figure 10 demonstrates the effect of  $\Sigma$  (inverse capillary number) on the stability of the system for the short-wave monotonic and oscillatory modes of instability. Following the similar trend with long-wave approximation (see Fig. 4), it can be observed that the stability of the system increases with increasing the magnitude of  $\Sigma$  for the short-wave perturbations as well. This is due to the enhanced dampening of surface

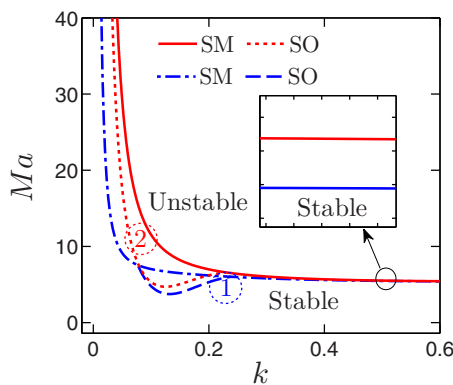


FIG. 8. Neutral stability curves for the short-wave monotonic (solid and dash-dotted lines) and oscillatory mode (dotted and dashed lines) for different values of  $Ga$  at  $Bi = 0.1$ ,  $Pr = 1$ , and  $\Sigma = 1000$ . Lines marked by 1 and 2 correspond to  $Ga = 1$  and  $Ga = 10$ , respectively. The inset shows the zoomed-in view of the neutral stability curve at higher wave number.

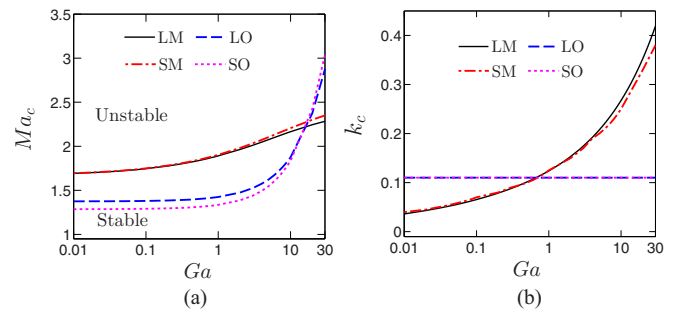


FIG. 9. (a) Variation of the critical Marangoni number and (b) the critical wave number with Galileo number at  $Bi = 0.05$ ,  $Pr = 1$ , and  $\Sigma = 1000$ . (a), (b), LM, LO, SM, and SO represent the long-wave monotonic, long-wave oscillatory, short-wave monotonic, and short-wave oscillatory modes, respectively.

deflection by the surface tension force for higher values of  $\Sigma$ . However, the increasing magnitude of  $\Sigma$  reduces the range of disturbance wave number ( $k$ ) for which the oscillatory mode is critical as can be verified from Fig. 10.

We show in Figs. 11(a) and 11(b) the variation of critical Marangoni number ( $Ma_c$ ) and disturbance wave number ( $k_c$ ) with the inverse capillary number ( $\Sigma$ ). From Fig. 11(a), it can be observed that, up to a certain critical value of  $\Sigma$  ( $\Sigma = 720$  corresponding to  $Bi\Sigma = 72$ ),  $Ma_c$  associated with the long-wave monotonic mode of instability increases, after which it becomes independent of  $\Sigma$ . This is because, for  $Bi\Sigma \geq 72$ , the neutral stability curve for the monotonic mode of instability attains the limiting value of  $Ma_c = 48Bi$  [see Eq. (23)]. However, at  $Bi\Sigma \geq 72$ ,  $Ma_c$  for the short-wave monotonic mode of instability slightly exceeds the value  $48Bi$  and it continues to grow marginally with  $\Sigma$ . Figure 11(a) further reveals that, for the set of parameters considered in the present plotting, the oscillatory mode is critical only for small values of  $\Sigma$ . Since the increasing magnitude of  $\Sigma$  reduces the deformability of the free surface, this further ascertains the fact that oscillatory instability occurs only for a deformable free surface. However, the range of  $\Sigma$  for which the oscillatory

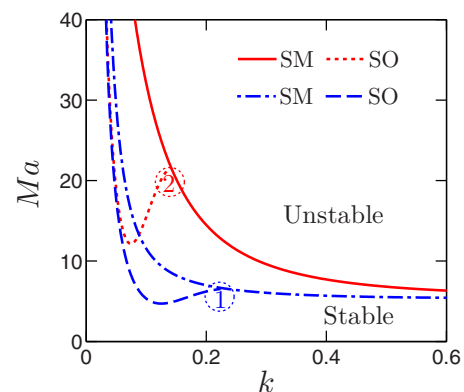


FIG. 10. Neutral stability curves for the short-wave monotonic (solid and dash-dotted lines) and oscillatory modes (dotted and dashed lines) for different values of  $\Sigma$  at  $Bi = 0.1$ ,  $Pr = 1$ , and  $Ga = 10$ . Lines marked by 1 and 2 correspond to  $\Sigma = 1000$  and  $\Sigma = 10000$ , respectively.

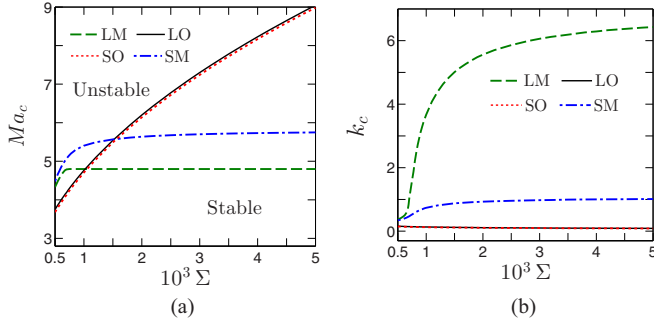


FIG. 11. Variation of (a) the critical Marangoni number and (b) the critical wave number with  $\Sigma$  at  $\text{Bi} = 0.1$ ,  $\text{Pr} = 1$ , and  $\text{Ga} = 10$ . (a), (b); LM, LO, SM, and SO represent the long-wave monotonic, long-wave oscillatory, short-wave monotonic, and short-wave oscillatory modes, respectively.

mode becomes critical is large for short-wave perturbations as compared to the long-wave perturbations.

We demonstrate in Fig. 11(b) the variation of  $k_c$  with  $\Sigma$ . From Fig. 11(b) one can find that, beyond a certain value of  $\Sigma$  ( $\Sigma = 720$  corresponding to  $\text{Bi}\Sigma = 72$ ),  $k_c$  for the long-wave monotonic mode increases rapidly, thus leaving the domain of applicability of long-wave approximation. Note that, for this particular value of  $\Sigma$  ( $= 720$ ), the neutral stability curve for the long-wave monotonic mode attains the limiting value of  $\text{Ma}_c = 4.8$  as depicted by Fig. 11(a).

Keeping in mind the verification of our theoretically predicted value with the results from possible experimentation, in particular, towards the possible validation of the theoretical modeling framework employed in this paper with the experimental results, in Fig. 12 we demonstrate the neutral stability curve for a real system comprising an aqueous 1-butanol solution. It is important to mention here that, upon heating, such a fluid layer presents a nonmonotonic variation of surface tension with temperature as verified from experimental observations of Villers and Platten [28]. From Fig. 12 we can observe that, for the chosen set of dimensionless parameters, the oscillatory mode is critical with  $\text{Ma}_c = 1.19$  at  $k_c = 0.06$ . For a fluid layer

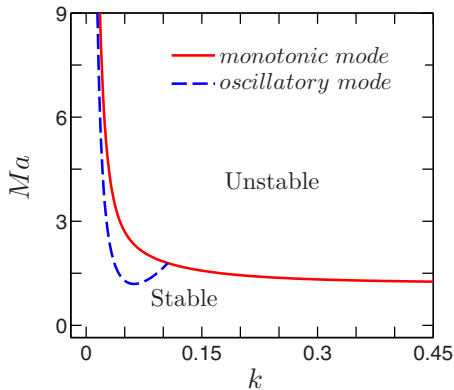


FIG. 12. Neutral stability curves for an aqueous 1-butanol fluid layer of thickness 0.05 mm,  $\text{Bi} = 0.025$ ,  $\text{Ga} = 6$ , and  $\Sigma = 5000$ . The solid line represents the monotonic mode, and dashed one corresponds to the oscillatory mode of instability.

of thickness 0.05 mm and  $\nu = 100$  cSt, this critical Marangoni number is achieved at a temperature difference of 6 K with characteristic wavelength of 0.5 mm. We would like to mention here that one can verify experimentally the neutral stability curve for both the monotonic and oscillatory modes for a liquid layer heated from below with the observations and the variations reflected in Fig. 12 as well as the theoretically predicted value of critical Marangoni number obtained for a magnitude of temperature difference 6 K.

### C. Model comparison with the previous studies

In this section, we make an attempt to compare our results with the earlier reported results in the literature for a system that has a close resemblance to the present system. We also discuss the implications of the nonmonotonic variation of surface tension on the stability of the system. For a liquid layer resting on an insulating substrate and heated from below, ShklyaeV *et al.* [48] investigated the Marangoni convection by considering the linear variation of surface tension with temperature for the long-wave perturbations. They obtain the following neutral stability curves for the monotonic and oscillatory modes of instability:

$$\text{Ma}_{L,m} = \frac{48(\text{Bi} + k^2)(\text{Ga} + \Sigma k^2)}{k^2(72 + \text{Ga} + \Sigma k^2)}, \quad (42)$$

$$\text{Ma}_{L,o} = 3 + \frac{3\text{Bi}}{k^2} + \text{Ga} + \Sigma k^2. \quad (43)$$

A comparison of the above equations [i.e., Eqs. (42) and (43)] with Eqs. (22) and (26) of the present analysis reveals that, for the nonmonotonic variation of surface tension with temperature,  $\text{Bi}$  (Biot number) appears as the correction factor in the expression for the neutral stability curve for both monotonic and oscillatory modes of instability. Symbolically it can be represented as  $\text{Ma} = \text{Bi}(\text{Ma}_L)$ . This is also true for the neutral stability curve for a liquid layer having a nondeformable free surface, for which we obtain  $\text{Ma} = 48\text{Bi}$  [in the limit of large  $k$ ; see Eq. (23)] compared to  $\text{Ma}_L = 48$  for the monotonic variation of surface tension with temperature [48]. Therefore, it is evident that, for Marangoni convection induced by nonmonotonic variation of surface tension with temperature, the stability of the system is significantly dependent on the Biot number (or the heat transfer rate) at the free surface. In this context, it is worth mentioning here that by complying with the earlier studies on Marangoni convection (where a monotonic variation of surface tension with temperature is considered [9]), for the present analysis also the stability of the system increases with increasing magnitude of  $\text{Bi}$  for both the long-wave and short-wave perturbations (see Figs. 2 and 5). Moreover, similar to the Marangoni convection induced by a linear variation of surface tension with temperature, for the nonmonotonic variation also, the oscillatory mode of instability occurs only for a deformable free surface [i.e., for small values of  $\text{Ga}$ ; see Fig. 7(b)].

## IV. CONCLUSIONS

In this paper, we have studied Marangoni convection in a thin liquid layer heated from below and separated from the surrounding gas phase by a deformable free surface.

Conducting this investigation, we aimed towards an understanding about the effect of nonmonotonic variation of surface tension (with temperature) on the onset of instability in the heated liquid layer for both the long-wave and short-wave perturbations. To analyze the Marangoni convection induced by such nonmonotonic variation of surface tension, here we define the quadratic Marangoni number (in contrast to the linear Marangoni number) to determine the stability of the liquid layer. For the long-wave Marangoni convection, using the scaling  $k \sim (\text{Bi})^{1/2}$ , we derive a set of amplitude equations [Eqs. (15) and (18)] that govern the coupled nonlinear evolution of the fluid layer thickness as well as temperature. Also, in this study, under the framework of linear stability analysis, we have analytically derived the neutral stability curve for the monotonic and oscillatory modes of instability for both long-wave and short-wave perturbations.

Compared to the earlier studies of Marangoni convection (see Shklyaev *et al.* [48], where a monotonic variation of

surface tension with temperature is considered) we have found that Bi (Biot number) appears as the correction factor in the expression for neutral stability curve, while accounting for a nonlinear variation of surface tension with temperature. It is found that such a nonlinear effect introduces a nontrivial change in the stability threshold of the liquid layer. The investigation reveals that, when such a fluid layer is heated from below, both monotonic and oscillatory instability can appear for a particular range of the dimensionless parameters, viz., Bi, Ga, and  $\Sigma$ . This study further demonstrates that increasing the magnitude of the above-mentioned parameters increases the stability of the fluid layer either by enhancing the heat transfer rate from the free surface or by reducing the surface deflection under the effect of gravity and surface tension. Finally, we found that, compared to the long-wave disturbance, the short-wave disturbance increases the range of the dimensionless parameters for which the oscillatory mode becomes critical.

#### APPENDIX: EXPRESSIONS FOR THE TERMS $\aleph_0 - \aleph_8$ APPEARING IN EQ. (41)

The terms  $\aleph_0 - \aleph_8$  appearing in Eq. (41) are defined by the following expressions:

$$\begin{aligned}\aleph_0 &= \gamma_1/\gamma_2, \\ \gamma_1 &= -\lambda \text{Pr} k_1^3 \cosh k_1 - 2\lambda \text{Pr} k_1 k^2 \cosh k + 3\lambda \text{Pr} k_1 k^2 \cosh k_1 + \lambda^2 k_1 \cosh k - \lambda^2 k_1 \cosh k_1 \\ &\quad + \text{Pr}(\text{Ga} + \Sigma k^2)(k k_1 \sinh k - k^2 \sinh k_1), \\ \gamma_2 &= 2\lambda \text{Pr} k^3 \sinh k + \lambda \text{Pr} k_1^3 \sinh k_1 - 3\lambda \text{Pr} k_1 k^2 \sinh k_1 - \lambda^2 k \sinh k + \lambda^2 k_1 \sinh k_1 \\ &\quad - \text{Pr} k^2 (\text{Ga} + \Sigma k^2)(\cosh k - \cosh k_1), \\ k_1 &= \sqrt{k^2 - \lambda/\text{Pr}}, \\ k_2 &= \sqrt{k^2 - \lambda}, \\ \aleph_1 &= \lambda k_2 \sinh k_2 + \lambda \text{Bi} \cosh k_2, \\ \aleph_2 &= -k k_1 \exp(-k_2) + \lambda k \exp(-k_2)/2k_1 + k k_1 \text{Bi} \exp(-k_2)/k_2 - \lambda \text{Bi} k \exp(-k_2)/2k_1 k_2 + k k_1 \cosh k \\ &\quad - \lambda k \sinh k_1/2 - \lambda k \cosh k_1/2k_1 + k \text{Bi} \sinh k_1 - \lambda \text{Bi} k \cosh k_1/2k_1, \\ \aleph_3 &= -\lambda \text{Bi} k \sinh k_1/2k_1 - \lambda k \cosh k_1/2 - \lambda k \sinh k_1/2k_1 + k^2 \sinh k + k \text{Bi} \sinh k_1, \\ \aleph_4 &= -2\text{Bi} \lambda k k_1 \sinh k + \text{Bi} \lambda k_1^2 \sinh k_1 + \text{Bi} \lambda k^2 \sinh k_1, \\ \aleph_5 &= -2\text{Bi} \lambda k^2 \cosh k + \text{Bi} \lambda k_1^2 \cosh k_1 + \text{Bi} \lambda k^2 \cosh k_1, \\ \aleph_6 &= -k^2 k_1 \exp(-k_2)/k_2 + \lambda k^2 \exp(-k_2)/2k_1 k_2 + \lambda k^2 \cosh k_1/2k_1 - k^2 \sinh k_1, \\ \aleph_7 &= \lambda k^2 \sinh k_1/2k_1 - k^2 \cosh k_1, \\ \aleph_8 &= \lambda k \cosh k_2.\end{aligned}$$

[1] M. G. Colinet, P. Legros, and J. C. Velarde, *Nonlinear Dynamics of Surface-Tension-Driven Instabilities* (Wiley, Berlin, 2001).  
[2] S. Davis, *Annu. Rev. Fluid Mech.* **19**, 403 (1987).  
[3] M. F. Schatz and G. P. Neitzel, *Annu. Rev. Fluid Mech.* **33**, 93 (2001).  
[4] B. J. Won, W. Lee, and S. Song, *Sci. Rep.* **7**, 3062 (2017).  
[5] M. Orlishausen, L. Butzhammer, D. Schlotzbohm, D. Zapf, and W. Köhler, *Soft Matter* **13**, 7053 (2017).

[6] R. H. Farahi, A. Passian, T. L. Ferrell, and T. Thundat, *Appl. Phys. Lett.* **85**, 4237 (2004).  
[7] D. A. Nield, *J. Fluid Mech.* **19**, 341 (1964).  
[8] J. C. Palmer, J. Harvey, and J. Berg, *Fluid Mech.* **47**, 779 (1971).  
[9] J. R. A. Pearson, *J. Fluid Mech.* **4**, 489 (1958).  
[10] C. Normand, Y. Pomeau, and M. G. Velarde, *Rev. Mod. Phys.* **49**, 581 (1977).

- [11] H. Kawamura, K. Nishino, S. Matsumoto, and I. Ueno, *J. Heat Transfer* **134**, 031005 (2012).
- [12] L. G. Napolitano, *Science* **225**, 197 (1984).
- [13] C. H. Chun and W. Wuest, *Acta Astronaut.* **5**, 681 (1978).
- [14] D. Schwabe, *Adv. Space Res.* **24**, 1347 (1999).
- [15] P. L. G. Ybarra, J. L. Castillo, and M. G. Velarde, *Phys. Fluids* **30**, 2655 (1987).
- [16] K. A. Cliffe and S. J. Tavener, *J. Comput. Phys.* **145**, 193 (1998).
- [17] A. Oron and P. Rosenau, *Phys. Rev. A* **39**, 2063 (1989).
- [18] J. A. Maroto, V. Pérez-Muñuzuri, and M. S. Romero-Cano, *Eur. J. Phys.* **28**, 311 (2007).
- [19] C. L. McTaggart, *J. Fluid Mech.* **134**, 301 (1983).
- [20] J. K. Bhattacharjee, *Phys. Rev. E* **50**, 1198 (1994).
- [21] A. Mikishev and A. A. Nepomnyashchy, *Colloids Surf., A* **521**, 161 (2017).
- [22] A. Oron and A. A. Nepomnyashchy, *Phys. Rev. E* **69**, 016313 (2004).
- [23] A. A. Shklyaev and S. Nepomnyashchy, *J. Fluid Mech.* **718**, 428 (2013).
- [24] M. Morozov, A. Oron, and A. A. Nepomnyashchy, *Phys. Fluids* **26**, 112101 (2014).
- [25] G. J. Gittens, *J. Colloid Interface Sci.* **30**, 406 (1969).
- [26] S. Shklyaev, M. Khenner, and A. A. Alabuzhev, *Phys. Rev. E* **82**, 025302(R) (2010).
- [27] M. Celli, A. Barletta, and L. S. de B. Alves, *Phys. Rev. E* **91**, 023006 (2015).
- [28] D. Villers and J. K. Platten, *J. Phys. Chem.* **92**, 4023 (1988).
- [29] S. Enders and H. Kahl, *Fluid Phase Equilib.* **263**, 160 (2008).
- [30] H. Zhou, Y. Zhu, T. Peng, Y. Song, J. An, X. Leng, Z. Yi, Y. Sun, and H. Jia, *J. Mol. Liq.* **223**, 516 (2016).
- [31] M. G. J. Gannon and T. E. Faber, *Philos. Mag. A* **37**, 117 (1978).
- [32] R. Aveyard, B. P. Binks, T. A. Lawless, and J. Mead, *J. Chem. Soc., Faraday Trans.* **81**, 2155 (1985).
- [33] J. Restolho, J. L. Mata, and B. Saramago, *J. Chem. Phys.* **134**, 074702 (2011).
- [34] Y. Abe, *Ann. N. Y. Acad. Sci.* **1077**, 650 (2006).
- [35] N. di Francescantonio, R. Savino, and Y. Abe, *Int. J. Heat Mass Transfer* **51**, 6199 (2008).
- [36] Y. Hu, S. Zhang, X. Li, and S. Wang, *Int. J. Heat Mass Transfer* **83**, 64 (2015).
- [37] N. Zhang, *Int. Commun. Heat Mass Transfer* **28**, 1025 (2001).
- [38] L. Y. Yeo, R. V. Craster, and O. K. Matar, *Phys. Rev. E* **67**, 056315 (2003).
- [39] J. C. Rednikov, A. Ye., P. Colinet, M. G. Velarde, and J. C. Legros, *J. Fluid Mech.* **405**, 57 (2000).
- [40] J. C. Legros, *Acta Astronaut.* **13**, 697 (1986).
- [41] A. Oron and P. Rosenau, *J. Fluid Mech.* **273**, 361 (1994).
- [42] W. Batson, Y. Agnon, and A. Oron, *J. Fluid Mech.* **819**, 562 (2017).
- [43] M. Takashima, *J. Phys. Soc. Jpn.* **50**, 2745 (1981).
- [44] M. C. Benguria and R. D. Depassier, *Phys. Fluids A* **1**, 1123 (1989).
- [45] M. Bestehorn and P. Colinet, *Phys. D (Amsterdam, Neth.)* **145**, 84 (2000).
- [46] E. A. Ryabitskii, *Fluid Dyn.* **28**, 3 (1993).
- [47] M. Takashima, *J. Phys. Soc. Jpn.* **50**, 2751 (1981).
- [48] S. Shklyaev, A. A. Alabuzhev, and M. Khenner, *Phys. Rev. E* **85**, 016328 (2012).
- [49] A. E. Samoilova and N. I. Lobov, *Phys. Fluids* **26**, 064101 (2014).
- [50] A. Podolny, A. A. Nepomnyashchy, and A. Oron, *Math. Modell. Nat. Phenom.* **3**, 1 (2008).
- [51] A. Oron, S. H. Davis, and S. G. Bankoff, *Rev. Mod. Phys.* **69**, 931 (1997).
- [52] A. A. Podolny, A. Oron, and A. Nepomnyashchy, *Phys. Fluids* **17**, 104104 (2005).
- [53] R. V. Craster and O. K. Matar, *Rev. Mod. Phys.* **81**, 1131 (2009).
- [54] A. Y. Rednikov, P. Colinet, M. G. Velarde, and J. C. Legros, *J. Non-Equilib. Thermodyn.* **25**, 381 (2000).